Do new data on $B^+ \to \tau^+ \nu_\tau$ decays point to an early discovery of supersymmetry at the LHC?

Biplob Bhattacherjee,[*] Amol Dighe,[†] Diptimoy Ghosh,[‡] and Sreerup Raychaudhuri[§]

Department of Theoretical Physics, Tata Institute of Fundamental Research, 1, Homi Bhabha Road, Mumbai 400 005, India

(Received 22 December 2010; published 20 May 2011)

The recent Belle and *BABAR* measurements of the branching ratio of $B^+ \to \tau^+ \nu_\tau$ indicate a significant deviation from the standard model prediction. We demonstrate that this measurement has a serious impact on models with minimal flavor violation involving a charged Higgs boson, ruling out a large portion of the currently allowed parameter space. In the constrained minimal supersymmetric standard model, this creates a tension between the measurements of $B^+ \to \tau^+ \nu_\tau$ and the anomalous magnetic moment of the muon, unless $\tan\beta$ is small, $\mu > 0$, and A_0 takes a large negative value. In fact, a very small region of the parameter space of this model, with small values of m_0 and $m_{1/2}$, survives all the constraints at 95% C.L. It is remarkable that this specific region is still consistent with the lightest supersymmetric particle as the dark matter. Moreover, it predicts observable supersymmetric signals in the early runs of the LHC, even perhaps at 7 TeV. We also show that a consistent explanation for the deviation of the $B^+ \to \tau^+ \nu_\tau$ branching ratio from the standard model can be achieved in a nonuniversal Higgs-mass model, which could also predict early signals of supersymmetry at the LHC.

DOI: 10.1103/PhysRevD.83.094026 PACS numbers: 13.20.He, 12.60.Jv, 14.80.Da

I. INTRODUCTION

Now that the CERN LHC has commenced its long-awaited run and the first physics results have been analyzed and made public [1,2], there is an atmosphere of palpable suspense in the high energy physics community as to what physics results will come out as more and more data are collected and studied, and most importantly, as to whether these results will indicate new physics (NP) beyond the standard model (SM). The experimental programme is more or less clear: more statistics will be accumulated, and the results will be compared with the predictions of the SM. Deviations from the latter would imply some sort of NP, and one can refer to existing theoretical studies to indicate what kind of NP is indicated by the observed deviation. It is true that theorists have not succeeded in providing an unequivocal prediction in this regard. This is because there exist several rival possibilities for NP, each with good arguments both for and against it. However, for several technical and aesthetic reasons, of which tractable ultraviolet behavior and the natural appearance of chiral fermions are perhaps the most important, supersymmetry (SUSY) has always been the pick of these NP models. At the dawn of the LHC era, it still remains the first option for any study of NP predictions.

Elegant as SUSY may be as an abstract idea, it is well known that it presents a very different face when it comes to constructing realistic models at low energies. Any phenomenologically viable SUSY model must necessarily include a large number of soft SUSY-breaking parameters. A count of the number of free phenomenological parameters in the so-called minimal supersymmetric standard model (MSSM) [3] runs to over 100, including masses, coupling constants, and mixing angles for the large number of supersymmetric partners, or sparticles, in the model. This proliferation of parameters may be directly traced to the fact that the MSSM does not include a specific mechanism for the breaking of SUSY, and hence, the numerous SUSY-breaking parameters are essentially put in by hand. Although such a model can exist, at least in principle, a theory with a hundred odd free parameters is a phenomenologist's nightmare, since it leads to very few clear predictions at the empirical level. At the LHC, for example, this leads to a wide landscape of possible signals which would leave an experimentalist with hard data to compare with a bewildering variety of options [4]. It is also difficult to believe that the breaking of SUSY is a sheer accident brought on by a proliferation of arbitrary nonzero parameters. One would rather argue that there is a definite mechanism for SUSY breaking [5], and when we know it, we will also know the parameters in question. Once again, however, theorists have failed to come up with an unambiguous mechanism for SUSY breaking—there exist quite a few different suggestions [6], beginning with minimal supergravity (mSUGRA) models, through gauge-mediated SUSY breaking, anomaly mediated SUSY breaking and so on, each with a very different pattern for the parameters in question. Each of these models has different predictions for LHC signals, and hence, in effect, the chaotic situation within the subset of SUSY models becomes a cameo of the general NP scenario.

The oldest, and perhaps the most restrictive, of these SUSY models where a specific mechanism for SUSY breaking is considered, is the so-called "constrained" MSSM (cMSSM), which is based on an underlying

[*]biplob@theory.tifr.res.in
[†]amol@theory.tifr.res.in
[‡]diptimoyghosh@theory.tifr.res.in
[§]sreerup@theory.tifr.res.in

mSUGRA [7] scenario.[1] In this scenario, supergravity is broken spontaneously in a so-called ''hidden'' sector consisting of fields which do not have strong or electroweak couplings to the MSSM fields. However, gravity, which necessarily couples to all fields so long as they carry energy and momentum, acts as a mediator between the hidden sector and the MSSM sector, giving rise to the soft SUSY-breaking parameters. It is this circumstance that leads to a dramatic reduction in the number of parameters, since gravity is blind to all flavor and color quantum numbers, though it can sense the spin of a particle. As a result, the mSUGRA model has just five free parameters, viz. (i) a universal scalar mass m_0, (ii) a universal fermion mass $m_{1/2}$, (iii) a universal trilinear (scalar) coupling A_0, (iv) the ratio of vacuum expectation values of the two Higgs doublets, parametrized as $\tan\beta$, and (v) the Higgsino mixing parameter μ. This universality of the masses and couplings is valid at the scale where the SUSY-breaking parameters are generated, which is usually identified with the scale of grand unification (GUT scale),[2] i.e., above 10^{16} GeV. While running down to low energies using the renormalization group (RG) equations, however, the various soft SUSY-breaking parameters evolve differently, and lead to a specific mass spectrum at the electroweak scale. In particular, one of the Higgs-mass-squared parameters is driven to a negative value, ensuring that the electroweak symmetry is spontaneously broken. The requirement that the electroweak symmetry be broken at precisely the right scale leads to a further constraint, which effectively fixes the magnitude of μ in terms of the other parameters, though its sign is still indeterminate. This version of the mSUGRA model, which depends on four parameters and a sign, viz. $\{m_0, m_{1/2}, A_0, \tan\beta, \mathrm{sgn}\mu\}$, is called the cMSSM. Being more constrained, this model is also more predictive and hence is more readily testable. There exists, therefore, a vast amount of literature on this model, which has been studied with regard to (a) collider signals [8], (b) low-energy processes, such as decays of K, D, and B mesons [9,10], and (c) dark-matter constraints arising from the fact that the relic density of the lightest SUSY particle (LSP) can be identified with the dark-matter content of the Universe [11]. In this article, therefore, we shall focus on this model, though a simple extension will also figure into our analysis.

It is now common knowledge that null results from direct searches have pushed up the masses of sparticles into the regime of 100 GeV or above. However, SUSY models can still make substantial contributions to low-energy processes, particularly those which are mediated by weak interactions. Among these, flavor-changing neutral current (FCNC) processes, with the famed Glashow-Iliopoulos-Maiani cancellation, constitute a favored ground to look for SUSY effects (or any NP effects, for that matter). However, barring a few little hiccups, the SM rules supreme in the area of flavor physics, leaving very little room for NP theories, including SUSY and the cMSSM. Year by year, as the measurements of the FCNC processes grow better and better, the lower bounds on masses of new particles (including sparticles) have been creeping further and further up in order to squeeze the NP contributions into the ever-narrowing band of experimental errors in these measurements.

In this article, we consider one such recent low-energy experimental result, viz., the measurement of the branching ratio $B^+ \to \tau^+ \nu_\tau$. It directly constrains all models with minimal flavor violation (MFV), viz., models where all flavor-changing transitions are entirely governed by the Cabibbo-Kobayashi-Maskawa (CKM) matrix with no new phases beyond the CKM phase δ. We find constraints on general NP with MFV that involves a charged Higgs boson. As the cMSSM (and almost any viable SUSY model) belongs to this category, we apply these constraints to the cMSSM and find a rather dramatic impact on the parameter space of the model. It turns out when we combine the results of the measurement in question with other low-energy measurements, such as the anomalous magnetic moment of the muon, and radiative and leptonic B decays, most of the cMSSM parameter space is disfavored at the 95% confidence level (C.L.). What survives all the constraints is a small patch in the four-dimensional parameter space $(m_0, m_{1/2}, A_0, \tan\beta)$ of the model, for a positive sign of μ. This is very different from the kind of constraints derived from earlier, less restrictive measurements of $B^+ \to \tau^+ \nu_\tau$, where wide areas of the cMSSM parameter space were allowed.

As mentioned above, one of the attractive features of SUSY is that it provides a dark-matter candidate, viz., the LSP. This carries a conserved quantum number (R parity) which forbids its decay.[3] One can, therefore, study the evolution of the Universe in a SUSY model, and check whether the relic density of LSP's matches with the observed density of dark matter as indicated by the cosmic microwave background radiation (CMBR) data [13]. Obviously, this matching will happen for only a small part of the parameter space of the model. It is encouraging that the dark-matter-allowed region in the cMSSM overlaps the small patch allowed by low-energy measurements quite substantially. We can say, therefore, that there exists a

[1]This mechanism, by invoking supergravity, gives up the good ultraviolet behavior, unless, indeed, the supergravity model is equivalent to, or embedded in, a string theory. Aficionados of the cMSSM would, of course, argue that gravity must eventually be included anyway.

[2]There exists a symbiotic relation between SUSY and grand unified theory (GUT) ideas, since SUSY solves the hierarchy problem in GUT, and a GUT is natural at the scale where SUSY breaking is generated.

[3]Once again, this is not written in stone, for R-parity violation can happen and has been extensively studied [12].

rather specific set of parameters which is simultaneously consistent with the low-energy data as well as with the hypothesis that LSP's form the dark-matter content of the Universe. With this specific set of parameters, we generate the mass spectrum of sparticles, and find reasonably unequivocal indications as to the kind of signals expected at the LHC. No detailed analysis is necessary at this stage, for the relevant signals have already been considered in comprehensive studies by the ATLAS and CMS Collaborations [14,15]. Comparing their results with our parameter choice, we find that the 7 TeV run of the LHC may provide a weak indication of SUSY [16], which could be verified comprehensively even in the very early stages of the 14 TeV run. Going further, we may even say that if SUSY is indeed the correct NP option, then the LHC may eventually turn out to be the hoped-for SUSY factory, claimed in the literature [17].

This article is organized as follows. In Sec. II we discuss the recent bounds on $B^+ \to \tau^+ \nu_\tau$ and how they affect MFV models. This is followed by Sec. III, where we discuss other low-energy measurements which constrain the cMSSM parameter space. The combined constraints are displayed and discussed in Sec. IV, where we also discuss the possible LHC signals which could arise therefrom. Section V discusses the so-called nonuniversal Higgs-mass (NUHM) model, a variant of the cMSSM, and some of its consequences. A critical summary of our results forms the substance of the concluding Sec. VI.

II. THE DECAY $B^+ \to \tau^+ \nu_\tau$

On purely theoretical grounds, the leptonic decay $B^+ \to \tau^+ \nu_\tau$ is a clean decay mode, since the final state consists only of leptons and hence the usually troublesome strong rescattering phases are absent. Indeed, in the SM, the branching ratio of $B^+ \to \tau^+ \nu_\tau$ is given by the tree-level formula

$$\mathrm{BR}(B^+ \to \tau^+ \nu_\tau)_{\mathrm{SM}} = \frac{G_F^2 m_B m_\tau^2}{8\pi}\left(1 - \frac{m_\tau^2}{m_B^2}\right)^2 f_B^2 |V_{ub}|^2 \tau_B, \tag{1}$$

where G_F is the Fermi constant, τ_B is the B^+ lifetime, $f_B = 192.8 \pm 9.9$ MeV [18] is the B^+ decay constant, and m_B, m_τ are the masses of B^+, τ^+, respectively. Here

$$|V_{ub}| = (3.52 \pm 0.11) \times 10^{-3} \tag{2}$$

is the relevant CKM matrix element, obtained through the combined fit [19,20] to all the data excluding the $B^+ \to \tau^+ \nu_\tau$ measurements. The SM prediction, including higher-order corrections, is

$$\mathrm{BR}(B^+ \to \tau^+ \nu_\tau)_{\mathrm{SM}} = (0.81 \pm 0.15) \times 10^{-4}. \tag{3}$$

As recently as 2008, the experimental average value of this parameter [21] was

$$\mathrm{BR}(B^+ \to \tau^+ \nu_\tau)_{2008} = (1.41 \pm 0.43) \times 10^{-4}, \tag{4}$$

which was just about consistent with Eq. (3) at 1 standard deviation. At that time, it was shown [22] that corresponding constraints on the parameter space of the cMSSM (such as we discuss in this work) are rather minor.

Very recently (2010), however, new measurements of the branching ratio $\mathrm{BR}(B^+ \to \tau^+ \nu_\tau)$ from B factories have changed the experimental value quite significantly. The most recent experimental measurements are [23–26]

$$\begin{aligned} BABAR\,(\text{semileptonic tag}):\ & \mathrm{BR}(B^+ \to \tau^+ \nu_\tau) = (1.70 \pm 0.82) \times 10^{-4}, \\ (\text{hadronic tag}):\ & \mathrm{BR}(B^+ \to \tau^+ \nu_\tau) = (1.80 \pm 0.61) \times 10^{-4}, \\ \text{Belle}\,(\text{semileptonic tag}):\ & \mathrm{BR}(B^+ \to \tau^+ \nu_\tau) = (1.54 \pm 0.48) \times 10^{-4}, \\ (\text{hadronic tag}):\ & \mathrm{BR}(B^+ \to \tau^+ \nu_\tau) = (1.79 \pm 0.71) \times 10^{-4}. \end{aligned} \tag{5}$$

These results are quite consistent with each other. Combining these measurements, one gets the world average [27]

$$\mathrm{BR}(B^+ \to \tau^+ \nu_\tau)_{\mathrm{exp}} = (1.68 \pm 0.31) \times 10^{-4}. \tag{6}$$

Clearly, this measurement deviates significantly from the SM prediction given in Eq. (3). Defining $R^{\mathrm{exp}}_{\tau\nu_\tau}$ to be [28,29]

$$R^{\mathrm{exp}}_{\tau\nu_\tau} \equiv \frac{\mathrm{BR}(B^+ \to \tau^+ \nu_\tau)_{\mathrm{exp}}}{\mathrm{BR}(B^+ \to \tau^+ \nu_\tau)_{\mathrm{SM}}}, \tag{7}$$

and using Eqs. (3) and (6), we get

$$R^{\mathrm{exp}}_{\tau\nu_\tau} = 2.07 \pm 0.54, \tag{8}$$

which indicates a $\sim 2\sigma$ deviation. Deviations at this level frequently arise from statistical fluctuations in small data samples, or from the use of ill-determined theoretical quantities, and often disappear when more data are analyzed, or when more rigorous calculations are performed. In this case, however, the mismatch may not disappear so easily. This is because the current measurements of $\mathrm{BR}(B^+ \to \tau^+ \nu_\tau)$ are not based on a small statistics sample (see Refs. [23–26]). Also, one should not expect the SM prediction to change much, since the formula in Eq. (1) involves quantities that are already known pretty accurately. It appears, therefore, that it is sensible to at least explore the ability of NP beyond the SM to resolve the observed discrepancy.

Following Ref. [28], we characterize the NP models that could potentially explain this anomaly by a quantity $R^{\rm NP}_{\tau\nu_\tau}$, defined as

$$R^{\rm NP}_{\tau\nu_\tau} \equiv \frac{{\rm BR}(B^+ \to \tau^+\nu_\tau)_{\rm SM+NP}}{{\rm BR}(B^+ \to \tau^+\nu_\tau)_{\rm SM}}, \tag{9}$$

where the subscript SM + NP represents the net branching ratio in the NP scenario, including the SM contribution. The 95% C.L. allowed range for $R^{\rm NP}_{\tau\nu_\tau}$ then works out to

$$0.99 < R^{\rm NP}_{\tau\nu_\tau} < 3.14, \tag{10}$$

which essentially means that NP models with positive contributions are favored by the data and those with negative contributions are quite strongly disfavored.

There exist, of course, a wide variety of models of NP which could provide extra contributions to the branching ratio of $B^+ \to \tau^+\nu_\tau$. However, we focus only on the MFV models. For a large class of MFV models that involve a charged Higgs boson H^+—such as two-Higgs doublet models, of which the cMSSM is an example—the branching ratio of $B^+ \to \tau^+\nu_\tau$ is given by [30]

$${\rm BR}(B^+ \to \tau^+\nu_\tau)_{\rm NP} = \frac{G_F^2 m_B m_\tau^2}{8\pi}\left(1 - \frac{m_\tau^2}{m_B^2}\right)^2 f_B^2 |\tilde{V}_{ub}|^2 \tau_B \times \left(1 - \tan^2\beta \frac{m_B^2}{M_+^2}\right)^2 \tag{11}$$

at the tree level, where M_+ is the mass of the charged Higgs boson. Here NP stands specifically for the MFV model, but we retain the notation "NP" in the interests of simplicity.[4]

In the above formula $|\tilde{V}_{ub}|$ is the value of $|V_{ub}|$ obtained in the context of the NP model, which, in general, will be different from $|V_{ub}|$ obtained from the data in the context of the SM. In order to get rid of this uncertainty in the CKM parameter, we restrict ourselves to the determination of $|V_{ub}|$ through only those measurements that are independent of NP. Such a fit is called the fit to the universal unitarity triangle (UUTfit) [31], and it uses only

(i) the measurements of $|V_{ub}/V_{cb}|$ from semileptonic B decays,
(ii) the ratio of mass differences in the B_s and B_d systems: $|\Delta M_s/\Delta M_d|$, and
(iii) the measurement of $\sin 2\beta$ from the time-dependent CP asymmetry in $B_d \to J/\psi K^{(*)}$.

The UUTfit value of $|V_{ub}|$ comes out as [19]

$$|V_{ub}|_{\rm UUTfit} = (3.50 \pm 0.12) \times 10^{-3}, \tag{12}$$

which is actually very close to the global fit in Eq. (2). Using this value, the SM prediction for the branching ratio of $B^+ \to \tau^+\nu_\tau$ changes slightly from Eq. (3) and becomes

$${\rm BR}\,(B^+ \to \tau^+\nu_\tau)_{\rm SM} = (0.80 \pm 0.15) \times 10^{-4}. \tag{13}$$

Note that while the UUTfit [19] is obtained using the lattice prediction $f_B = 200 \pm 20$ MeV [32] of the LQCD Collaboration, we use the more recent, averaged value from lattice simulations, $f_B = 192.8 \pm 9.9$ MeV [18], which has a much smaller error,[5] for the calculation of ${\rm BR}(B^+ \to \tau^+\nu_\tau)_{\rm SM}$. The 95% C.L. allowed range for $R^{\rm NP}_{\tau\nu_\tau}$ assumes the value

$$0.99 < R^{\rm NP}_{\tau\nu_\tau} < 3.19, \tag{14}$$

which forms the basis of all subsequent analyses in this article. Once $|V_{ub}|$ is chosen in this "model-independent" way, we can take $|\tilde{V}_{ub}| = |V_{ub}|_{\rm UUTfit}$, and hence the theoretical MFV prediction for $R^{\rm NP}_{\tau\nu}$ at the tree level becomes

$$R^{\rm NP}_{\tau\nu_\tau}|_{\rm tree} = \left(1 - \tan^2\beta \frac{m_B^2}{M_+^2}\right)^2. \tag{15}$$

If higher-order corrections are included then this ratio gets modified [33] to a form

$$R^{\rm NP}_{\tau\nu_\tau} = \left(1 - \frac{\tan^2\beta}{1 + \tilde{\epsilon}_0 \tan\beta} \frac{m_B^2}{M_+^2}\right)^2, \tag{16}$$

where $\tilde{\epsilon}_0$ encodes all the higher-order corrections, which, of course, will have some dependence on the free parameters of the MFV model. We take the range of $\tilde{\epsilon}_0$ to be $-0.01 \le \tilde{\epsilon}_0 \le 0.01$, as obtained in [34] by a scan over reasonable values of the MFV model parameters. When a specific model, such as the cMSSM, is considered, $\tilde{\epsilon}_0$ can be calculated explicitly.

The impact of the experimental data on MFV models with a charged Higgs boson, as discussed above, can be clearly discerned from Fig. 1(a), where we plot the value of $R^{\rm NP}_{\tau\nu_\tau}$ as a function of the charged Higgs boson mass M_+. As Eq. (14) indicates, such a model should tend to make $R^{NP}_{\tau\nu_\tau}$ greater than unity, and there is very little room for $R^{NP}_{\tau\nu_\tau} < 1$. However, the negative sign on the right side of Eq. (16) indicates that unless the NP contribution is very large, the models in question have a tendency to diminish $R^{\rm NP}_{\tau\nu_\tau}$ rather than augment its value. As a result, a model with a heavy charged Higgs boson *cannot* be considered as an explanation for the deviation of ${\rm BR}(B^+ \to \tau^+\nu_\tau)$ from its SM value. Instead, if we do have such a model, we would expect rather strong constraints on its parameters, since the NP contribution must be squeezed into the small tolerance below unity, as given in Eq. (14). Such a situation would naturally arise for large M_+, when the NP

[4]Note that our analysis for the MFV models in this section closely follows that of [19], with minor differences. Our constraints in the $M_+ - \tan\beta$ parameter space naturally are almost identical. However, we present the detailed analysis here for the sake of completeness and clarification of our procedure.

[5]Ideally, of course, the UUTfit needs to be performed again with the updated f_B value. We have assumed that the updated fit will not significantly affect the $|V_{ub}|$ value.

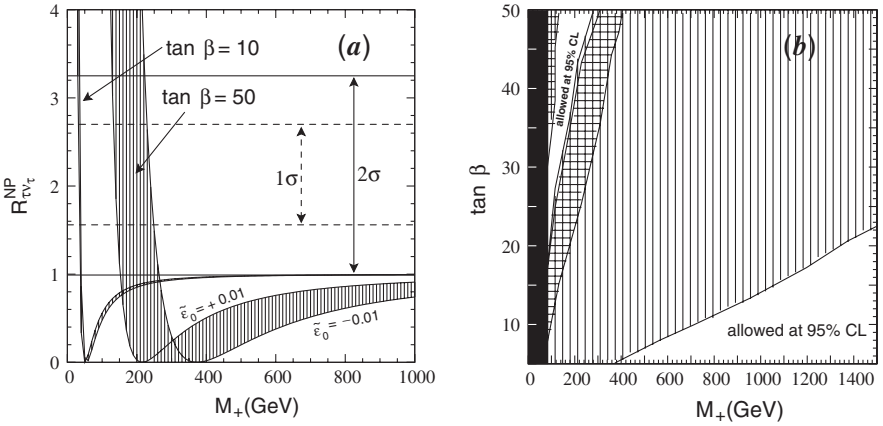

FIG. 1. (a) The dependence of $R^{\rm NP}_{\tau\nu_\tau}$ on the mass M_+ of the charged Higgs boson in MFV models for two values $\tan\beta = 10$ and 50, and (b) the 95% C.L. constraints on the $M_+ - \tan\beta$ plane. The vertically hatched regions in (a) correspond to higher order corrections varying between $\tilde{\epsilon}_0 = -0.01$ and $+0.01$, while the 1σ (2σ) experimental measurements of $R^{\rm NP}_{\tau\nu_\tau}$ are shown by horizontal broken (solid) lines. The dark band in (b) corresponds to the LEP bound. The large, vertically hatched region in (b) is disallowed by the recent (2010) $R^{\rm NP}_{\tau\nu_\tau}$ constraint, while the horizontally hatched region is disallowed by the 2008 data.

contribution becomes negligible, and $R^{\rm NP}_{\tau\nu_\tau} \to 1$ for all $\tan\beta$—though it always stays less than unity. This corresponds to the rising part of the curves, towards the right end of Fig. 1(a). A glance at the figure will, however, leave no doubt that this limiting case is barely allowed at 2σ for low $\tan\beta(= 10)$, but disallowed for high $\tan\beta(= 50)$. We surmise, therefore, that for high values of M_+, the $B^+ \to \tau^+ \nu_\tau$ measurement favors low values of $\tan\beta$.

For low values of M_+, on the other hand, Eq. (16) tells us that it is possible for the NP contribution to be so large that it completely dominates the SM contribution, and in this limit, it is possible to have $R^{\rm NP}_{\tau\nu_\tau} \gtrsim 1$. The explicit condition is

$$\frac{\tan^2\beta}{1 + \tilde{\epsilon}_0 \tan\beta} \gtrsim \frac{2M_+^2}{m_B^2}. \tag{17}$$

However, this can happen only for a very restricted set of $(M_+, \tan\beta)$ values, some of which are already constrained experimentally. For example, for $\tan\beta = 10$, one can have $R^{\rm NP}_{\tau\nu_\tau}$ well inside the 2σ range only if M_+ is $\lesssim 50$ GeV, but such low M_+ values are ruled out by the LEP direct searches, which give $M_+ > 79.3$ GeV [35]. On the other hand, if $\tan\beta = 50$, the same LEP data permit 140 GeV $< M_+ < 220$ GeV which can render $R^{\rm NP}_{\tau\nu}$ well inside the 2σ range, as shown in Fig. 1(a). Thus, one may complement our earlier assertion by the statement that in the opposite limit, i.e. for low values of M_+, the $B^+ \to \tau^+ \nu_\tau$ measurement favors high values of $\tan\beta$. This is also the limit in which the NP models contribute positively in accounting for the deviation of the experimental data from the SM predictions.

The two limits are made explicit in Fig. 1(b), which shows the 95% C.L. constraints on the $M_+ - \tan\beta$ plane. The dark band represents the LEP constraint $M_+ > 79.3$ GeV and the vertically hatched region is disallowed by the $B^+ \to \tau^+ \nu_\tau$ measurement. This leaves only two small unshaded regions for low M_+ and high M_+, in accordance with the above discussion. Our result may be contrasted with the constraints obtained from the 2008 data, which are shown by horizontal hatching, and constrain only a small region with $M_+ < 400$ GeV and somewhat high $\tan\beta$. One may say, therefore, that the recent measurement of the branching ratio for $B^+ \to \tau^+ \nu_\tau$ has considerably improved the constraints on MFV models with charged Higgs bosons. As the cMSSM belongs to this category, we should expect correspondingly severe constraints on the corresponding parameter space when we compare its predictions with this new experimental result.

III. OTHER CONSTRAINTS

When we consider an all-encompassing model like the cMSSM, with far-flung implications in almost all areas of electroweak physics, the constraints arising from $B^+ \to \tau^+ \nu_\tau$ cannot be considered in isolation, but must be combined with other bounds—some of which are equally restrictive, at least at the 2σ level. These constraints can be classified as follows.

(1) *Theoretical constraints*.—arising from requirements of internal consistency of the model. In particular, if the Higgs-mass parameter which should be driven negative by RG running remains positive, we cannot explain electroweak symmetry breaking (EWSB) in this model. There is also a substantial region where the model predicts that the charged stau $\tilde{\tau}_1$ is the LSP, and is therefore precluded by the absence of a large relic density of charged particles.

(2) *Collider bounds*.—arising from the nondiscovery in direct searches [35] at the CERN LEP and Fermilab Tevatron of predicted particles, most notably the

light Higgs boson h^0 and the lighter chargino $\tilde{\chi}_1^+$. While the chargino couplings are large enough for the experimental bounds to practically saturate the kinematic reach of these machines, the light Higgs boson mass in SUSY models is generally sensitive to higher-order corrections, where there is a theoretical uncertainty of around 3–4 GeV at the next-to-next-to-leading order and higher [36]. To take care of this, we consider a softer lower bound of 111 GeV, rather than the kinematic bound of 114.4 GeV usually applied to the SM Higgs boson.

(3) *Indirect bounds*.— arising from measurements of low-energy processes where new particles and interactions in NP models can also contribute. In the context of the cMSSM, the most important of these are the measurements of (a) the anomalous magnetic moment of the muon, (b) the rate of the radiative decay $B_d \to X_s\gamma$, and (c) the BR for the leptonic decay $B_s \to \mu^+\mu^-$. Here we have assumed that the NP is of the MFV kind, and that it survives the measurements other than those explicitly mentioned above. In particular, the large $B_s - \bar{B}_s$ mixing phase, or the $A_{CP}(B \to K\pi)$ measurements, cannot be explained by any MFV models, and we assume that these anomalies will disappear with more data or with better theoretical calculations.

Of the above, the theoretical and direct search constraints may be considered firm constraints, as they are unlikely to be changed by inclusion of further types of NP along with the cMSSM or whatever model is being studied. On the other hand, constraints from indirect measurements are not so robust, as they can easily change if some new effect is postulated. Before we proceed to apply these constraints to the cMSSM parameter space, therefore, a brief discussion of the actual measurements used in our analysis is called for. This forms the remaining part of this section.

(i) *The anomalous magnetic moment of the muon*, $a_\mu = (g-2)/2$: This is one of the most compelling indicators of NP and it is well known as a major constraint for NP theories such as supersymmetry or extra dimensions. The latest measured value [37] for a_μ is

$$a_\mu^{\rm exp} = (11\,659\,208.0 \pm 6.3) \times 10^{-10}. \quad (18)$$

In the recent past, the SM prediction [31] for a_μ has undergone numerous vicissitudes with respect to the experimental data, occasionally being consistent with them and occasionally deviating at the level of 2σ–3σ. Much of the difficulty in making this prediction accurate lies in the fact that the experimental measurement is sensitive to two-loop corrections where some nonperturbative QCD effects due to the low mass scale are involved. The latter have to be obtained by fitting experimental data, whose errors then feed into the theoretical uncertainty. The most recent SM prediction is [38]

$$a_\mu^{\rm SM} = (11\,659\,178.5 \pm 6.1) \times 10^{-10}. \quad (19)$$

The discrepancy between the SM and experiment is, therefore,

$$\Delta a_\mu^{\rm exp} = a_\mu^{\rm exp} - a_\mu^{\rm SM} = (29.5 \pm 8.8) \times 10^{-10}. \quad (20)$$

This is at the somewhat high level of $\sim 3.4\sigma$, but is not normally considered a "smoking gun" signal for NP for reasons stated above. Nevertheless, in order to check if this discrepancy *can* be explained with the cMSSM, we use a procedure [39] that does not calculate the two-loop SUSY corrections, but includes them in the theoretical errors, to obtain a 95% C.L. range

$$11.5 \times 10^{-10} < \Delta a_\mu^{\rm NP} < 47.5 \times 10^{-10}, \quad (21)$$

where $\Delta a_\mu^{\rm NP}$ is the extra contribution due to NP. In our analysis, the NP in question will be the cMSSM, or a variant, but we choose, as in the previous section, to retain the label "NP."

Obviously, in the cMSSM, the value of $\Delta a_\mu^{\rm NP}$ will depend on all the free parameters of the model. However, it is known that the sign of the cMSSM contribution is directly sensitive to the sign of the μ parameter [40]: for $\mu < 0$, the cMSSM contribution is negative, while for $\mu > 0$, a positive contribution is predicted by some regions of the cMSSM parameter space. Since the 95% C.L. range of $\Delta a_\mu^{\rm NP}$ indicated in Eq. (21) is entirely positive, it indicates that the sign $\mu < 0$ is disallowed by the measurement of the muon anomalous magnetic moment, and even with $\mu > 0$, there are strong constraints on the remaining parameters of the cMSSM.

(ii) *The radiative decay* $B_d \to X_s\gamma$: In the SM, the BR of the radiative decay $B_d \to X_s\gamma$ has been calculated [41] to next-to-next-to-leading order in QCD to be

$$\mathrm{BR}\,(B_d \to X_s\gamma)_{\rm SM} = (3.15 \pm 0.23) \times 10^{-4}. \quad (22)$$

The current experimental average for the BR by the Heavy Flavor Averaging Group [42] is

$$\mathrm{BR}\,(B_d \to X_s\gamma)_{\rm exp} = (3.55 \pm 0.26) \times 10^{-4}, \quad (23)$$

which is consistent with the SM prediction within 1 standard deviation, leaving very little room for NP contributions. As a result, this measurement has a tremendous impact on MFV models involving a charged Higgs boson H^+, essentially pushing up the mass M_+ to very large values. Of all such models, the constraints on SUSY models can be more relaxed because of large cancellations

between the charged Higgs boson contributions and the chargino contributions which are the hallmark of SUSY models. Nevertheless, there do exist bounds on the cMSSM arising from the residual contribution, especially for light M_+, and these have to be taken into consideration.

In our analysis, after including the theoretical uncertainties in the cMSSM following the method outlined in [29], we set the 95% C.L. range for the branching ratio to be

$$2.05 \times 10^{-4} \leq \mathrm{BR}(B_d \to X_s \gamma) \leq 5.05 \times 10^{-4}. \tag{24}$$

It turns out that the $B_d \to X_s \gamma$ constraint is also extremely sensitive to the sign of μ. For $\mu < 0$, it eliminates a large part of the parameter space [43], while for $\mu > 0$ the constraint is comparatively weaker. Neither of these constraints is as strong as those arising from the muon $(g-2)/2$; however, they are complementary to it.

(iii) *The leptonic decay* $B_s \to \mu^+ \mu^-$: Within the SM, the fully leptonic decay $B_s \to \mu^+ \mu^-$ is chirally suppressed; the SM prediction is

$$\mathrm{BR}\,(B_s \to \mu^+ \mu^-)_{\mathrm{SM}} = (3.19 \pm 0.35) \times 10^{-9}. \tag{25}$$

The uncertainty in the BR comes principally from the decay constant $f_{B_s} = 238.8 \pm 9.5$ MeV [18] and from the CKM element $|V_{ts}| = 0.041 \pm 0.001$ [35]. The current experimental upper bound by the CDF Collaboration is [44]

$$\mathrm{BR}\,(B_s \to \mu^+ \mu^-)_{\mathrm{CDF}} < 4.3 \times 10^{-8} (95\%\ \mathrm{C.L.}). \tag{26}$$

After including the theoretical uncertainties, we get the 95% C.L. upper limit

$$\mathrm{BR}\,(B_s \to \mu^+ \mu^-) < 4.8 \times 10^{-8}. \tag{27}$$

Inclusion of charged Higgs bosons, whose left- and right-chiral couplings depend on $\cot\beta$ and $\tan\beta$, respectively, has a direct impact on the BR for $B_s \to \mu^+ \mu^-$, which gets enhanced considerably above the SM prediction, and easily saturates the upper bound, especially for low values of M_+ and large $\tan\beta$. Indeed, for large $\tan\beta$, the cMSSM contribution is known [45] to scale as $\tan^6\beta/(M_+^2 - M_W^2)^2$. Thus, this process also constrains MFV models with a charged Higgs boson. It turns out that for the cMSSM, these constraints are not more severe than the combination of all other constraints; however, we shall demonstrate later that they do have an impact if the assumptions of the cMSSM are relaxed.

In this section, we have listed the major constraints, apart from the new data on $B^+ \to \tau^+ \nu_\tau$, on the parameter space of SUSY models, of which the cMSSM will be showcased in the following section. It may be noted in passing that this list is not fixed for all time, as there are several other low-energy processes and direct search bounds which also constrain the SUSY parameter space. Current data on these rule out patches of the parameter space which are subsumed in the disallowed regions arising from the constraints which we have listed above. However, it is entirely possible that a future measurement—including some LHC searches—could rule out wider patches of the SUSY parameter space, and then the relevant processes would have to be taken into consideration. With this caveat, we now turn to the explicit constraints on the cMSSM parameter space, and the impact of the $B^+ \to \tau^+ \nu_\tau$ measurement on this analysis.

IV. CONSTRAINING THE CMSSM

As mentioned in the Introduction, the parameter space of the cMSSM has four unknowns, viz. m_0, $m_{1/2}$, A_0, $\tan\beta$, that can take real values. The sign of the μ parameter is also undetermined, but as indicated in the previous section, the muon $(g-2)/2$ constraint disfavors $\mu < 0$. We therefore restrict ourselves to $\mu > 0$ and, hence, consider a simply connected parameter space of four dimensions.

The theoretical ranges of the parameters m_0, $m_{1/2}$, and A_0 are, in principle, completely undetermined, but the region of interest is clearly that which would lead to sparticle masses kinematically accessible to current accelerators such as the LHC. Keeping this in mind, we scan the ranges

$$\begin{aligned} 0 \leq m_0 &\leq 2\ \mathrm{TeV}, \\ 0 \leq m_{1/2} &\leq 1\ \mathrm{TeV}, \\ -2\ \mathrm{TeV} \leq A_0 &\leq 2\ \mathrm{TeV}. \end{aligned} \tag{28}$$

The range of the remaining parameter $\tan\beta$ is determined mainly by its impact on the scalar Higgs sector of the cMSSM, where, indeed, it arises. For very low values of $\tan\beta$ (~ 1), one tends to predict the lightest Higgs boson h^0 to have a small mass, which is already ruled out by the LEP constraints. On the other hand, if $\tan\beta > m_t/m_b$, the couplings of the charged Higgs boson to a $t\bar{b}$ pair begin to enter the nonperturbative regime. We have chosen, therefore, the reasonable range

$$4 \leq \tan\beta \leq 50. \tag{29}$$

Using these parameters, we perform a numerical scan over the cMSSM parameter space, using (a) SUSPECT [46] to generate the mass spectrum (this also takes care of the theoretical and direct search constraints), (b) SUPERISO [47] to calculate the variables listed as indirect constraints in the previous section, and, finally, (c) MICROMEGAS [48] to calculate the dark-matter relic density. All of these are

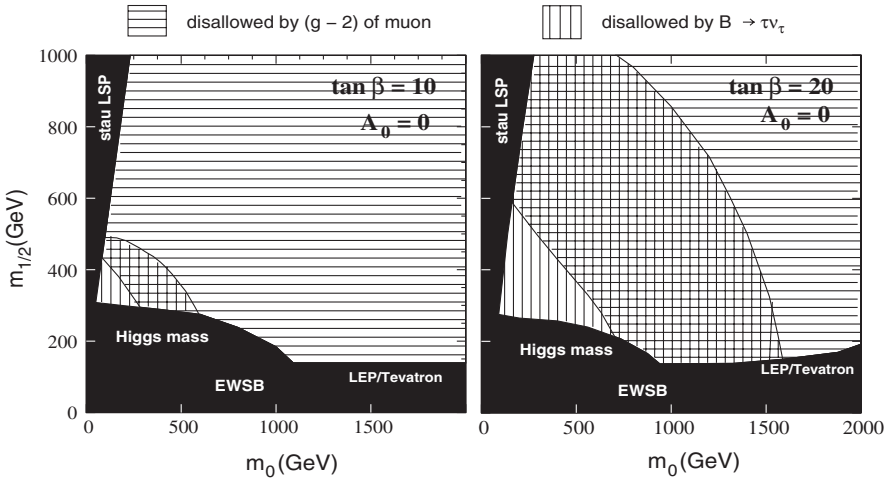

FIG. 2. The 95% C.L. constraints on the $m_0 - m_{1/2}$ plane, for $A_0 = 0$ and $\tan\beta = 10$ (left panel) and $\tan\beta = 20$ (right panel). Horizontal (vertical) hatching indicates regions ruled out by the measurement of the muon $(g-2)/2$ [BR$(B^+ \to \tau^+\nu_\tau)$], and the cross-hatched region represents their overlap. The constraint from $B \to X_s\gamma$ is subsumed in that from the lower bound on the Higgs mass from direct searches, and hence is invisible in these plots. We take $\mu > 0$ in this and all subsequent plots.

state-of-the-art software in the public domain, guaranteed to include higher-order corrections as available at the moment, which have been tested in multifarious applications, as the literature testifies.

In Fig. 2, we present the constraints on the cMSSM parameter space in the $m_0 - m_{1/2}$ plane, where the tension between various measurements appears quite clearly. For this figure, we have set $A_0 = 0$, which is an assumption commonly made for simplicity. We take $\mu > 0$ as required by the muon $(g-2)/2$ constraint. The panel on the left (right) corresponds to $\tan\beta = 10(20)$. The dark areas are ruled out by the theoretical and direct search constraints explained in the previous section, with the approximate areas highlighted in white lettering.[6] Focusing on the left panel, it is clear that the muon $(g-2)/2$ constraint (indicated by horizontal hatching) is very stringent, ruling out almost all the region considered, and allowing only a small patch with low values of m_0 and $m_{1/2}$. This patch, however, is disallowed by the new measurement of $B^+ \to \tau^+\nu_\tau$, as can be seen from the vertical hatching. The overlap between the disallowed regions is indicated by cross-hatching. It is quite clear, therefore, that for $\tan\beta = 10$, there is *no* region in the parameter space shown that is at once consistent (to 95% C.L.) with both the anomalous muon magnetic moment and the $B^+ \to \tau^+\nu_\tau$ branching ratio. We have checked that even if we take $\tan\beta$ down to values as small as $\tan\beta = 4$, the two measurements, taken together with the firm constraints, do not allow for a simultaneously allowed parameter space. At higher values of $\tan\beta$, the situation is even worse. This is apparent from the right panel, where our results are plotted for $\tan\beta = 20$. Here it is true that a larger region is permitted by the muon $(g-2)/2$ measurement, but the region disallowed by the $B^+ \to \tau^+\nu_\tau$ branching ratio is also much larger and covers the entire region allowed by $(g-2)/2$. The region disallowed by $B^+ \to \tau^+\nu_\tau$ grows for larger values of $\tan\beta$, as may be guessed from Fig. 1(b), and for values of $\tan\beta \sim 50$, it would cover the whole of the parameter space shown in the panels of Fig. 2. Thus, for $A_0 = 0$, one may say that these two measurements alone are enough to ensure that the full mSUGRA parameter space is strongly disfavored.

It may be noted in passing that among the other constraints from the low-energy data, the patch disallowed by $B_d \to X_s\gamma$ is subsumed in that from the Higgs-mass bound, and, likewise, the patch inconsistent with $B_s \to \mu^+\mu^-$ is overlaid by the dark region corresponding to the firm constraints. We have not, therefore, shown these disallowed regions in Fig. 2.

The above result, disappointing as it may appear, is by no means the end of the road for the cMSSM, for it has been obtained only on the slice of parameter space for which $A_0 = 0$. The situation changes when we permit A_0 to vary. This affects the running of the charged Higgs boson mass, and we find that for large negative values of A_0, for a given $\tan\beta$, the Higgs mass M_+ is driven to larger values than what one would obtain by setting $A_0 = 0$. In the context of Fig. 1(b), this effect then pushes the model horizontally in the $M_+ - \tan\beta$ plane, eventually penetrating into the "allowed" region. The $B^+ \to \tau^+\nu_\tau$ constraint, therefore, can be quite considerably weakened by choosing large negative values of A_0. We do not expect such a significant change in the muon $(g-2)/2$ constraint, but some relaxation is not unreasonable to expect when A_0 is varied over a wide range. Large negative values of A_0 also tend to increase the mass of the lightest Higgs boson h^0,

[6]Following common practice, we do not delineate separate patches in the firmly disallowed (dark) region in detail, as that would not be germane to the present discussion.

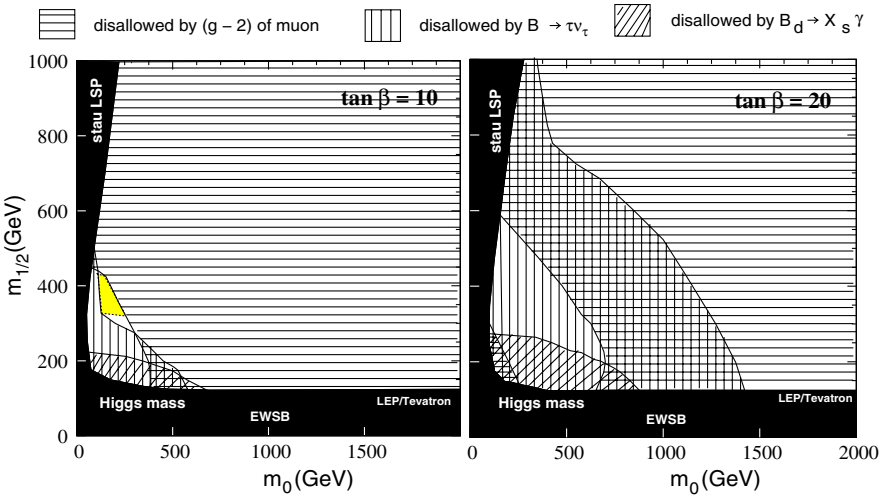

FIG. 3 (color online). The same as in Fig. 2, except that the trilinear coupling A_0 is kept floating over the range $(-2, +2)$ TeV, and regions are considered disallowed only if they remain disallowed for all values of A_0 in the given range. This weakens the constraints enough for a small allowed region to appear in the left panel ($\tan\beta = 10$). The yellow/light gray region is simultaneously consistent with *all* constraints at 95% C.L.

thereby relaxing somewhat the LEP bounds arising from Higgs boson mass considerations [49]. Accordingly, we repeat our analysis of the constraints on the $m_0 - m_{1/2}$ plane, keeping A_0 floating between -2 TeV and $+2$ TeV. In our analysis, a point in the $m_0 - m_{1/2}$ plane, for a given $\tan\beta$, is taken to be allowed at 95% C.L. by a given constraint if we can find any value of A_0, lying in the range -2 TeV $\leq A_0 \leq 2$ TeV, for which the given constraint is satisfied. Our results are exhibited in Fig. 3, which follows the notations and conventions of Fig. 2 closely. In addition to the constraints shown therein, the one from $B_d \to X_s\gamma$ now makes its appearance as a small region hatched with slanting lines, indicating that this constraint is now stronger than the weakened Higgs-mass bound from collider machines. However, it is not strong enough to rule out any portion which is not already disallowed by the other constraints.

Even a cursory examination of the dark and hatched regions in Fig. 3 will indicate that, while the qualitative features of the regions disfavored by the muon $(g-2)/2$ and the $B^+ \to \tau^+ \nu_\tau$ measurements stay the same, somewhat larger areas in the plane are ''allowed'' by each constraint individually. This, by itself, is not surprising, but it has the exciting consequence that now the left panel ($\tan\beta = 10$) exhibits a small patch, roughly triangular in shape, which satisfies each of the constraints individually for *some* value of A_0, and moreover, there is a subset of this region where all the constraints are satisfied simultaneously for the *same* value of A_0. This subregion, which represents the actual parameter space consistent with all the measurements individually at 95% C.L., is denoted by yellow/light gray shading. It is on this ''allowed'' region that we focus our interest in the subsequent discussion.

If we glance at the right panel of Fig. 3, where $\tan\beta = 20$, we see that there is no allowed region at all, the disallowed regions showing substantial overlap and covering the whole of the plot area. Once again, we surmise that high values of $\tan\beta$ are disfavored, whatever value of A_0 is chosen, and that the allowed region in the cMSSM parameter space must lie in the neighborhood of $\tan\beta = 10$. We have already mentioned that consistency with the $B^+ \to \tau^+ \nu_\tau$ constraint requires large negative values of the A_0 parameter, which can drive M_+ to higher values even for the low $\tan\beta(\approx 10)$. In order to see this, we plot, in the left panel of Fig. 4, the same constraints in the plane of A_0 and $m_{1/2}$, keeping m_0 fixed at the value $m_0 = 150$ GeV, for $\tan\beta = 10$. This particular value of m_0 has been chosen since in the left panel of Fig. 3, it lies, more or less, near the center of the allowed triangle (yellow/light gray shading) and is roughly the value for which the maximum range of $m_{1/2}$ appears to be allowed. The dimensions of this allowed triangle also encourage us, in Fig. 4, to ''zoom in'' on the range $m_{1/2} = 300$–500 GeV, outside which we get disallowed regions. However, A_0 is varied between -1.5 TeV and $+1.5$ TeV, to adequately cover the whole range allowed by the firm constraints, as is apparent from the left panel of Fig. 4.

It is immediately apparent from the left panel of Fig. 4 that about half of the region with positive values of A_0 is ruled out by the firm constraints, and the remaining half by the $B^+ \to \tau^+ \nu_\tau$ measurement. The latter has a severe impact on the $A_0 < 0$ region as well, essentially forcing us to consider large negative values of A_0 for small values of $m_{1/2}$. Including the muon $(g-2)/2$ constraint, which disfavors large values of $m_{1/2}$, then clinches the issue, permitting only another small wedge-shaped (yellow/light gray) region allowed by all the constraints. The maximum

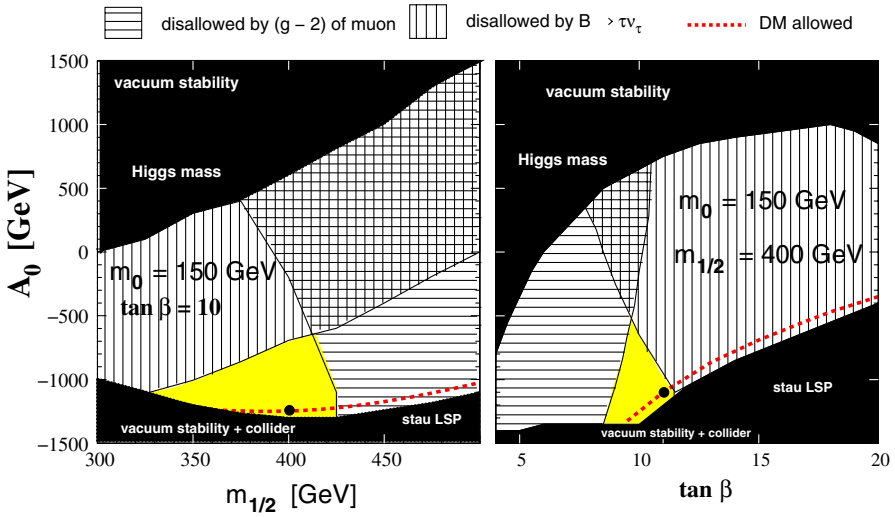

FIG. 4 (color online). Further constraints on the cMSSM parameter space. The left panel shows constraints on the $m_{1/2} - A_0$ plane, for $m_0 = 150$ GeV and $\tan\beta = 10$. The right panel shows, similarly, constraints on the $\tan\beta - A_0$ plane for $m_0 = 150$ GeV and $m_{1/2} = 400$ GeV. Notations and conventions are the same as in Figs. 2 and 3. The dotted (red) line represents the dark-matter-compatible region, and the black dot superposed on it is a benchmark point chosen for LHC studies.

range of $m_{1/2}$ permitted by all the constraints is around 325–425 GeV, which matches tolerably well with the vertical limits of the allowed triangle in Fig. 3, as should be the case. The value A_0, on the other hand, is quite strictly restricted to the approximate range -625 GeV to -1.4 TeV.

Of course, the above results are only for a fixed value $\tan\beta = 10$. Though we have already seen that jumping to a much larger value $\tan\beta = 20$ does not lead to any allowed region, it is interesting to zoom in to the $\tan\beta - A_0$ plane and see the impact of all these constraints there. This is shown in the right panel of Fig. 4, where we set $m_0 = 150$ GeV as before, and $m_{1/2} = 400$ GeV, which lies close to its value on the left panel for which the allowed range of A_0 is maximum. Once again, the combined constraints predict a small allowed region, with a maximum range of $\tan\beta$ lying roughly between 8 and 12. If we now refer to Fig. 1(b), this means that the charged Higgs boson is predicted to have a mass $M_+ > 600$ GeV.

Combining all these results, therefore, we obtain a roughly polyhedral allowed region in the four-dimensional parameter space, which is enclosed in a rather small hypercube with sides approximately at

$$100\,\text{GeV} \lesssim m_0 \lesssim 225\,\text{GeV}, \quad 375\,\text{GeV} \lesssim m_{1/2} \lesssim 425\,\text{GeV},$$
$$-1.4\,\text{TeV} \lesssim A_0 \lesssim -625\,\text{GeV}, \quad 8 \lesssim \tan\beta \lesssim 12. \tag{30}$$

The volume of the actual allowed region is considerably smaller than that of the hypercube, given that the two-dimensional projections shown in the previous two figures are roughly triangular in shape. Compared to the large regions considered in traditional work on the cMSSM, this constitutes a rather specific region of parameter space, and encourages us to make specific predictions based on this model. One can easily argue that the qualitative features of the mass spectrum and couplings will not undergo dramatic changes from one end to the other of so small a box as this one, unless, indeed, it encloses some point(s) of instability. This is unlikely, for none of the many studies of the cMSSM parameter space have ever shown such a possibility.

The very first prediction one would naturally demand from a specific point or region in the cMSSM parameter space is whether this can adequately explain the dark-matter content of the Universe as a relic density of LSP's. The CMBR data indicate a relic density $\Omega h^2 = 0.1123 \pm 0.007$ at 95% C.L. [13]. In general, SUSY models with a low-lying mass spectrum, such as the one in question, tend to predict too large a density of LSP's unless these are coannihilated by some reaction with a substantial cross section. This leads to a restriction on the cMSSM parameter space, which, given the accuracy of the CMBR data, confines us, more or less, to a line passing through the four-dimensional parameter space. The dark-matter requirement is known to favor large negative values of A_0 [50], and it is rather gratifying to see that this line passes right through the allowed region in the parameter space discovered in this work—which seems to indicate that a SUSY explanation of dark matter may indeed be the correct one. The line consistent with the dark-matter requirement[7] is shown by red dots on both panels in Fig. 4 and may be

[7]We do not go so far as to call it a constraint, though this is not unheard of in the literature.

seen to pass clearly through the allowed region, favoring a narrow range of A_0 around -1.25 TeV and $\tan\beta$ in the range 9–11. This region is rather close to the forbidden stau LSP region, as is apparent in both panels of Fig. 4. In the allowed region, the lighter stau $\tilde{\tau}_1$ is rendered very light due to the presence of a large negative $m_\tau A_\tau$ in the off-diagonal terms in the stau mixing matrix; however, it is marginally heavier than the neutralino $\tilde{\chi}_1^0$ LSP. This permits stau coannihilation with neutralinos, and reduces the relic density so that it is within the observed range.

We note that there does not seem to be any *a priori* reason for the region allowed by the low-energy constraints to match with the dark-matter-compatible region, since the low-energy constraints come from processes quite different from those that control the relic density. Nevertheless, the fact that the two regions do show some overlap encourages us to argue that we are now converging on the correct region in the hitherto-unknown parameter space. We may, therefore, make bold as to venture some predictions regarding the collider signals for this range of parameter space, especially in the context of the LHC.

In order to make a clear prediction about the LHC signals, we choose the following benchmark point in the cMSSM parameter space:

$$\begin{aligned} &m_0 = 150 \text{ GeV}, && m_{1/2} = 400 \text{ GeV}, \\ &A_0 = -1250 \text{ GeV}, && \tan\beta = 10, \qquad \mu > 0. \end{aligned} \tag{31}$$

Not only does this lie inside the hypercube marked out in Eq. (30), but it lies well within the allowed region, and right on the line corresponding to the dark-matter requirement. In Fig. 4, this benchmark point is indicated by a small black circle in both panels [on top of the dotted (red) line labeled ''dark-matter'']. The mass spectrum and signals expected for this ''golden point'' will be typical of the entire allowed region, which is, after all, rather small. At this benchmark point, we get the central values of the observables to be $\mathrm{BR}(B \to X_s\gamma) = 2.64 \times 10^{-4}$, $R_{\tau\nu}^{\mathrm{NP}} = 0.993$, and $a_\mu = 13.0 \times 10^{-10}$. Clearly, all of these are consistent with the measurements to within 2σ, though $R_{\tau\nu}^{\mathrm{NP}}$ only barely survives the 2σ bound.

Let us first discuss the cMSSM mass spectrum expected with this benchmark point. We calculate[8] the mass spectrum and the branching ratios using the code SUSY-HIT [51] and taking $m_t = 173.1$ GeV. The lightest Higgs boson h^0 is predicted to have a mass around 119 GeV, which is consistent with current bounds, but lies precisely in the range where its detection is most problematic because of large QCD backgrounds at the LHC. In fact, a light Higgs boson of this mass range must be detected through the rare decay $h^0 \to \gamma\gamma$, which is unlikely in the 7 TeV run, and will require the accumulation of a fair amount of statistics even in the 14 TeV run. The heavy Higgs bosons, including the H^+, will lie in the range 835–840 GeV, which is again kinematically inaccessible in the 7 TeV run, but may be detectable at 14 TeV. We have already shown that for $\tan\beta = 10$, as taken for this benchmark point, this high value of M_+ is what allows us to evade the $B^+ \to \tau^+ \nu_\tau$ constraint. Turning now to sparticles, the LSP $\tilde{\chi}_1^0$ will have a mass of 164 GeV, with the next-to-LSP (NLSP) being, as expected, the $\tilde{\tau}_1$ with a mass of 171 GeV. As explained above, the closeness in these masses permits the coannihilation of stau, so that the relic density is controlled. In this scenario, this stau and the lightest neutralino are the only sparticles with masses below that of the top quark, all other particles being heavier. The nearly degenerate lighter chargino $\tilde{\chi}_1^+$ and second neutralino $\tilde{\chi}_2^0$ lie at 315 GeV, while the other sleptons and the sneutrinos have different masses in the 200–320 GeV range. The gluino mass, however, is as high as 934 GeV and the squark masses mostly populate the range 800–900 GeV, except for the $\tilde{b}_1$, with mass around 719 GeV, and a light stop $\tilde{t}_1$ which lies as low as 393 GeV.

An immediate consequence of these large squark and gluino masses is that the sparticle production cross section at the LHC will be on the low side: at 7 TeV it will be around 0.4 pb at LO, while at 14 TeV, it will have the much healthier value of 5.2 pb at LO. About 60% of these cross sections come from squark pair production, of which roughly half is due to $\tilde{t}_1\tilde{t}_1^*$ production alone. The $\tilde{t}_1$ will decay to a top quark and a neutralino with a BR $\sim 2/3$, and hence, a possible signal would be a top-enriched final state with large missing transverse energy (MET). However, the enormous $t\bar{t}$ background to this process must be taken into consideration when studying this signal. The other traditional signals for SUSY—cascade decays of the gluino or squarks to charginos and heavy neutralinos, ending up in multileptons, jets, and MET—in this case provide τ-rich final states because of the low-lying $\tilde{\tau}_1$. However, τ's coming from the decay $\tilde{\tau}_1 \to \tau + \tilde{\chi}_1^0$ will generally be too soft for detection, because of the small splitting $M(\tilde{\tau}_1) - M(\tilde{\chi}_1^0) \simeq 7$ GeV. Final states involving other charged leptons will be suppressed. This indicates that the best option to seek SUSY with this benchmark point is the final state with four or more jets and substantial MET, which can arise from cascade decays involving only strongly interacting sparticles and the invisible LSP.

In Fig. 5 we show the allowed parameter space (yellow/light gray) in the $m_0 - m_{1/2}$ plane for $\tan\beta = 10$ and floating A_0 (as in Fig. 3), and also the ATLAS 5σ discovery limit [52] at the 7 TeV run with an integrated luminosity of 1 fb^{-1}, using the four jets + MET channel. It may be seen that the entire parameter space allowed by low-energy constraints at 95% C.L., including our golden point, lies just outside the 5σ discovery limit of ATLAS. The ATLAS study, in fact, has shown that at neighboring points, an overall cross section of about 1 pb is required for a 5σ

[8]The masses obtained using different RG evolution algorithms differ by a few GeV, and the errors from the calculation are difficult to quantify. Here we give the exact values obtained by SUSY-HIT.

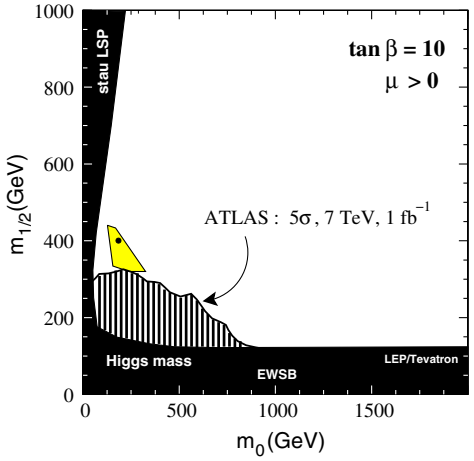

FIG. 5 (color online). The $m_0 - m_{1/2}$ plane in the cMSSM, showing the allowed region (yellow/light gray) for floating A_0, as well as the 5σ reach of the ATLAS detector at the 7 TeV run, using the jets + MET signal. The black dot inside the allowed region is the golden point discussed in the text. The entire nonshaded region inside this plot is accessible to the LHC with $\sqrt{s} = 14$ TeV with a luminosity of 10 fb^{-1}.

discovery using the four jets + MET channel. Making a simpleminded scaling with the predicted cross section of 0.4 pb at our benchmark point, one may expect a signal in this channel at the level of about 2σ. The same conclusions can be reached using the CMS 95% exclusion plot for the 7 TeV run [4]. Thus, by the end of 2011, as per the LHC running schedule, we may begin to see tantalizing hints of SUSY. If this should occur, then, in the 14 TeV run, it will be easy to see a 5σ signal with even 1 fb^{-1} of data—which should collect within the first few months. Interestingly, some of the direct production modes for charginos, which are electroweak in nature, lie at the level of 5%–10% of the total cross section. These may be difficult to detect in the 7 TeV run, but in the 14 TeV run, they are sure to provide additional signals for SUSY. With such copious production of sparticles, the LHC could indeed act as a SUSY factory, as mentioned in the Introduction.

V. NONUNIVERSAL HIGGS-MASS MODEL: EXPLAINING $B^+ \to \tau^+ \nu_\tau$

In the previous analysis, we have seen that the combination of constraints on the cMSSM parameter space leads to the prediction of a small value of $\tan\beta$ and hence, according to Fig. 1(b), the charged Higgs boson is necessarily heavy. Comparison with Fig. 1(a) readily shows that in this limit, the model is only just consistent with the $B^+ \to \tau^+ \nu_\tau$ constraint at 95% C.L. However, if we take the position that the 2σ discrepancy between the SM and the experimental result should be *explained* by a positive NP contribution, then the cMSSM fails the test, for it actually tends to diminish the SM prediction, and barely survives exclusion in a decoupling limit. This bare survival, by the skin of its teeth, as it were, is the proximate cause of the stringent constraints on the cMSSM parameter space discussed in the previous section.

As the cMSSM is the SUSY model with the maximum number of simplifying assumptions (and hence the minimum number of free parameters), it is interesting to ask if the relaxation of one or more of these assumptions could lead to a SUSY model which actually explains, rather than merely remains consistent with, the $B^+ \to \tau^+ \nu_\tau$ discrepancy. Since the NP effect in $B^+ \to \tau^+ \nu_\tau$ involves the scalar sector of the cMSSM, an obvious option would be to consider a model where the parameters of the Higgs sector are given a greater degree of flexibility than in the highly constrained cMSSM. In this context, an obvious choice of model is the so-called nonuniversal Higgs-mass (NUHM) model, which is an extension of the cMSSM where the Higgs-mass parameters m_{H_1} and m_{H_2} are delinked from the universal scalar mass parameter m_0 at the GUT scale and are allowed to vary freely [53]. At the electroweak scale, these two extra parameters m_{H_1} and m_{H_2} are usually traded for the Higgsino mixing parameter μ and the pseudoscalar Higgs boson mass m_A. This model, therefore, has *six* parameters, viz. m_0, $m_{1/2}$, μ, M_A, A_0, and $\tan\beta$.

NUHM models have been studied rather extensively, and various constraints on the six-dimensional parameter space have been found and exhibited in the literature [10,39,54]. What interests us here is the fact that M_A is a free parameter in the model, and it can be easily exchanged for M_+, to which it is related by the well-known SUSY relation

$$M_+^2 = M_A^2 + M_W^2, \tag{32}$$

at tree level. We can accordingly fix m_0, $m_{1/2}$, A_0, etc. at whatever value is required to satisfy the other constraints in the cMSSM, and then claim an explanation for the $B^+ \to \tau^+ \nu_\tau$ discrepancy by choosing a low M_+ and a high $\tan\beta$—this freedom being allowed by the bigger parameter space in the theory. However, large values of $\tan\beta$ and small values of M_+ lead to large charged Higgs boson-mediated contributions to the FCNC process $B_s \to \mu^+ \mu^-$, thus restricting the freedom in choosing parameter values. Here, as explained earlier, SUSY cancellations between the charged Higgs boson-mediated and the gaugino-mediated contributions come to the rescue: stringent bounds can be evaded if the gaugino masses are somewhat low, comparable to that of the light charged Higgs boson H^+. This, in turn, demands that the universal gaugino mass $m_{1/2}$ be somewhat small, compared with the other parameters, which are not so restricted.

While an exhaustive study of the NUHM parameter space *vis-à-vis* the present set of constraints would require a separate work in itself, it is interesting to see if the NUHM model can at all provide regions in parameter space which are consistent with all the constraints, and

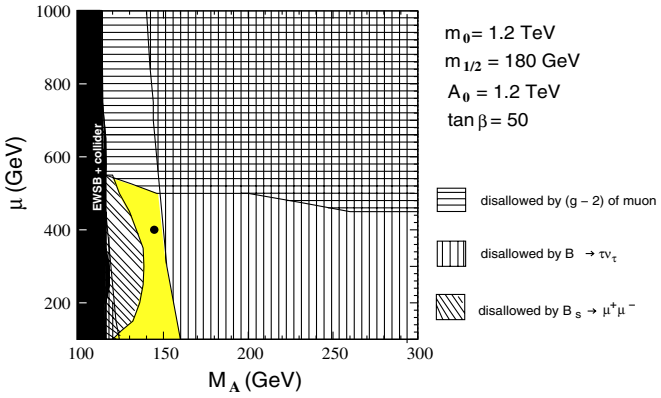

FIG. 6 (color online). Constraints on the $M_A - \mu$ parameter space in the NUHM model. Notations and conventions are the same as in the previous plots, except that now there is a significant constraint from $B_s \to \mu^+ \mu^-$ rather than $B_d \to X_s \gamma$. The yellow/light gray region is allowed by all the constraints, and the black dot inside it is a benchmark point chosen for LHC studies.

can simultaneously provide a NP explanation of the $B^+ \to \tau^+ \nu_\tau$ discrepancy. To illustrate that this is, in fact, possible, we show in Fig. 6 the regions allowed by the different constraints in the $m_A - \mu$ plane, keeping all the other parameters fixed at

$$\begin{aligned} m_0 &= 1.2 \text{ TeV}, \qquad m_{1/2} = 180 \text{ GeV}, \\ A_0 &= 1.2 \text{ TeV}, \qquad \tan\beta = 50. \end{aligned} \tag{33}$$

A glance at the figure will reveal that here, as in the cMSSM, there is a complementarity between the $B^+ \to \tau^+ \nu_\tau$ constraint and the $(g-2)/2$ constraint, the former tending to rule out larger values of M_A and the latter tending to rule out larger values of μ, as a result of which only a small rectangular patch in the $m_A - \mu$ plane is allowed by both constraints taken together. A large portion of this remaining patch is again disallowed by the $B_s \to \mu^+ \mu^-$ constraint, leaving a roughly sickle-shaped yellow/light gray region. In this region, M_A remains in the approximate range 100–150 GeV; i.e. M_+ lies roughly in the range 125–170 GeV, according to Eq. (32). Figure 1 then tells us that this is not only consistent with the experimental data, but it is precisely the range for which the NP explanation saturates the gap between the SM prediction and the experimental central value.

As before, to be precise about the LHC signals, we choose a benchmark point, which has the fixed parameter choices of Eq. (33) as well as

$$M_A = 145 \text{ GeV}, \qquad \mu = 400 \text{ GeV}, \tag{34}$$

which is indicated in Fig. 6 by a small black dot in the middle of the allowed (yellow/light gray) patch. The central values of the observables at this point are $\text{BR}(B \to X_s \gamma) = 3.5 \times 10^{-4}$, $R_{\tau\nu}^{\text{NP}} = 1.24$, $\text{BR}(B_s \to \mu^+ \mu^-) = 3.22 \times 10^{-8}$, $a_\mu = 12.8 \times 10^{-10}$, all of which are well within the 2σ range of the respective measurements. We note that the relic density of LSP's at this point is not enough to saturate the CMBR requirements, which means that this model is not ruled out by the latter, but is not a solution to that problem either.

The major features of the mass spectrum at this benchmark point are as follows: the lightest Higgs boson lies just beyond the LEP disallowed region, at 112 GeV, and, as in the cMSSM, this is a difficult mass range to search for the lightest Higgs boson. We would have to wait for enough statistics to accumulate at the 14 TeV run to see this Higgs boson in the $\gamma\gamma$ channel. The H^0 and A^0 lie at 145 GeV and may just be detectable through their decays to WW^* modes, while the charged Higgs boson H^+ lies at 170 GeV, where it will decay to $\tau^+ \nu_\tau$. These may also be detectable fairly early in the 14 TeV run. The LSP, as before, is the lightest neutralino $\tilde{\chi}_1$ with a mass of 71 GeV, which is permitted by the LEP direct search bound as applied to the NUHM [35]. The $\tilde{\chi}_1^+$ and $\tilde{\chi}_2^0$ lie at around 130 GeV, while the other gauginos are heavier than 400 GeV. The sleptons and squarks in this model are very heavy, lying in the range 700 GeV to 1.2 TeV, but the gluino $\tilde{g}$ is comparatively light, having a mass of 511 GeV.

As a consequence of the low-lying gaugino states contrasted with heavy sfermions, the dominant sparticle production channels in this model turn out to be to chargino pairs $\tilde{\chi}_1^+ \tilde{\chi}_1^-$ ($\sim 50\%$) and chargino-neutralino pairs $\tilde{\chi}_1^\pm \tilde{\chi}_2^0$ ($\sim 25\%$), with gluino pairs $\tilde{g}\,\tilde{g}$ bringing up the rear ($\sim 20\%$). The total cross section in this model would be 4.4 pb at 7 TeV and 27.3 pb at 14 TeV, i.e. much larger than the earlier case of the cMSSM. The gluino production channel can give rise to the same jets + MET signal as before, as each gluino will undergo three-body decays through virtual squarks. The production cross section for $\tilde{g}\,\tilde{g}$ pairs at 7 TeV is around 0.8 pb, which indicates that the jets + MET signal may actually be observable in the 7 TeV run at the 3σ–4σ level when 1 fb^{-1} of data have been collected. At 14 TeV, of course, a few hundred pb^{-1} of data would be enough to obtain a 5σ signal in this channel. Turning now to the chargino production modes, the rate of production of $\tilde{\chi}_1^+ \tilde{\chi}_1^-$ indicates a cross section for a dilepton + MET signal around 90 fb, which may not be discernible above the background, especially as the mass splitting $M(\tilde{\chi}_1^+) - M(\tilde{\chi}_1^0)$ is rather small. However, the $\tilde{\chi}_1^\pm \tilde{\chi}_2^0$ channel could lead to hadronically quiet trilepton + MET signals at the level of 74 fb, which have smaller SM backgrounds and hence could probably be seen as more data are collected in the 7 TeV run, and would be a sure-shot option at the 14 TeV run.

Before concluding this section, we reiterate that NUHM models which explain the $B^+ \to \tau^+ \nu_\tau$ discrepancy and, at the same time, remain consistent with the data on $B_s \to \mu^+ \mu^-$, will generically come with light gauginos, and lead to collider signals somewhat similar to those discussed

above. However, what we have studied is just one portion of the NUHM parameter space, inasmuch as we fixed m_0 and A_0 to very large values. A more comprehensive scan over the NUHM parameter space might reveal more patches consistent with all the constraints, and some of these may lead to collider signals which are different from those discussed in the context of our benchmark point. The detailed exploration of the NUHM parameter space in this context calls for a separate study.

VI. CONCLUDING REMARKS

With the commissioning of the LHC, the search for new physics beyond the standard model has assumed paramount importance in particle physics at the high scale. However, low-energy observables from flavor physics, like those from the decays of K, D, or B mesons, can offer indirect constraints on high scale physics. Indeed, with the high statistics available at the B factories *BABAR* and Belle, the freedom available for new physics has been substantially constrained. Most of the low-energy measurements have been consistent with the SM, and hence allow only a little leeway for NP. On the other hand, it is seen that the handful of measurements that indicate a $\sim 2\sigma$ deviation from the SM also restrain the NP parameters from taking arbitrary values.

In this paper, we have shown that the combined effect of both these kinds of low-energy measurements—those consistent with the SM (e.g. the branching ratios of $B_d \to X_s\gamma$ and $B_s \to \mu^+\mu^-$) as well as those showing deviations from the SM (e.g. the anomalous magnetic moment of the muon, and the branching ratio of $B^+ \to \tau^+\nu_\tau$)—results not only in indicating new physics, but also in pinpointing the relevant new physics parameters. In particular, we have pointed out that the latest measurement of the $B^+ \to \tau^+\nu_\tau$ branching ratio has a large impact on a large class of NP models, especially those which include a charged Higgs boson H^+. In fact, the decay $B^+ \to \tau^+\nu_\tau$, by itself, can constrain most of the models with minimal flavor violation that involve an H^+. This is because the latest measurement gives a branching ratio $\sim 2\sigma$ more than the SM prediction. If this discrepancy is to be explained by a MFV model, one needs very light charged Higgs bosons ($M_+ \lesssim 200$ GeV) and large $\tan\beta$ ($\gtrsim 20$). On the other hand, a heavy charged Higgs boson ($M_+ \gtrsim 300$ GeV) and a small $\tan\beta$ can be barely consistent with the data to within 2σ, but cannot be considered an explanation for the gap between theory and experiment. This is a general result that can be applied to any member of the MFV models, and we choose to apply it to the constrained MSSM, which is motivated by mSUGRA and is one of the most predictive SUSY models.

In cMSSM models, the charged Higgs boson is typically heavy, so that only the low $\tan\beta$ region survives the $B^+ \to \tau^+\nu_\tau$ measurement. When combined with the anomalous magnetic moment of the muon, the fate of even this region is in jeopardy: indeed, for a vanishing universal trilinear coupling A_0, there is no region in the cMSSM parameter space that is consistent with both these measurements to 95% C.L. The situation can only be salvaged with a large and negative A_0, and that too for an extremely small region in the $m_0 - m_{1/2}$ plane. The combined low-energy data thus pinpoint us to a very specific location (the golden point) in the five-dimensional parameter space of cMSSM: $\mu > 0$, $A_0 \approx -1.25$ TeV, $\tan\beta \approx 10$, $m_0 \approx 150$ GeV, $m_{1/2} \approx 400$ GeV, with a spread not more than that given in Eq. (30). It is remarkable that for part of this specific region, including the golden point, the mass and coupling of the LSP are exactly such that it can account for all the dark matter in the Universe. This may either be a coincidence or an indication that we are on the right track in our quest.

If we indeed are on the right track, and the golden point of the cMSSM is actually the NP that we have all been looking for, then we may not have to wait too long for its discovery. Since the values of m_0 and $m_{1/2}$ at this point are rather small, at the LHC, one expects a weak 2σ signal in the jets + MET channel even in the 7 TeV run with 1 fb^{-1} of integrated luminosity, and a 5σ discovery early in the 14 TeV run with just 1 fb^{-1} of data.

While the above suggestive coincidence is quite appealing, and the prospects of the detection of SUSY during the early parts of the 14 TeV run quite enticing, even at the golden point the model barely survives the 95% limit bounds and does not offer any help at all in explaining the $B^+ \to \tau^+\nu_\tau$ data—the absence of a light H^+ makes it impossible for the cMSSM to do so. We therefore explore a related but less constrained model, the NUHM, where the charged Higgs boson mass can be considered to be a free parameter. Here the presence of an extra parameter works wonders for explaining the low-energy data, covering the entire experimentally allowed region, including the central value. This model can also lead to rather spectacular trilepton + MET signals at the LHC, which may become detectable even towards the end of the 7 TeV run.

While our work tends to indicate a rather specific region of parameter space and specific signals at the LHC, especially for the cMSSM, there are some caveats which need to be taken into consideration, even apart from theoretical issues in the construction of the cMSSM. The first is the issue of experimental errors on the low-energy measurements, which we have taken at the 2σ level. If these are given more latitude (e.g. taken at the 3σ level) the constraints from low-energy processes would be considerably relaxed. In particular, the $B^+ \to \tau^+\nu_\tau$ measurement would still allow wide regions in the cMSSM parameter space. However, it would still disfavor very large values of $\tan\beta \sim 50$. A more serious point is the asymptotic behavior $R^{\rm NP}_{\tau\nu_\tau} \to 1$ in the large M_+ limit, as compared to the 2σ bound $R^{\rm NP}_{\tau\nu_\tau} > 0.99$. The strong constraint on NP comes because one must squeeze the contribution of the charged Higgs bosons into the narrow region 0.99–1.00. A small

downward revision in the lower bound on $R^{\rm NP}_{\tau\nu_\tau}$ could allow large $\tan\beta$ values even for large M_+. Such deviations can come from a variety of sources, such as higher-order corrections, a slightly changed value of f_B or $|V_{ub}|$, or a revised experimental result. On the other hand, a small upward revision of the allowed $R^{\rm NP}_{\tau\nu_\tau}$ band could rule out the entire gamut of MFV models with $M_+ > 200$ GeV. In particular, even the small leeway allowed for the cMSSM would then be closed. We note, therefore, that the bounds and predictions presented in this paper are specific to the experimental limits as they stand at present.

We have not made a very detailed study of the LHC signals, confining ourselves to generalities, because it is somewhat premature, at this stage, to make very definite predictions in this regard. Nevertheless, our work has highlighted the fact that if indeed we are to accept the cMSSM at face value, as most LHC studies do, then we should take the cMSSM in its entirety, i.e. all constraints from all sectors, including the low-energy sector. The next year and the years after it will be the most crucial in determining if our analysis, in fact, is on the right track.

ACKNOWLEDGMENTS

We would like to thank G. Mohanty (Belle Collaboration) for initiating a discussion on $B^+ \to \tau^+ \nu_\tau$ at WHEPP-XI.

[1] CMS Collaboration, https://twiki.cern.ch/twiki/bin/view/CMSPublic/PhysicsResults.
[2] ATLAS Collaboration, https://twiki.cern.ch/twiki/bin/view/Atlas/AtlasResults/Physics_Groups.
[3] H. P. Nilles, Phys. Rep. **110**, 1 (1984); H. E. Haber and G. L. Kane, *ibid.* **117**, 75 (1985); S. P. Martin, arXiv:hep-ph/9709356; M. E. Peskin, arXiv:0801.1928.
[4] P. Konar, K. T. Matchev, M. Park, and G. K. Sarangi, Phys. Rev. Lett. **105**, 221801 (2010).
[5] J. Wess and J. Bagger, *Supersymmetry and Supergravity* (Princeton University, Princeton, NJ, 1991), 2nd ed.
[6] M. Dress, R. M. Godbole, and P. Roy, *Theory and Phenomenology of Sparticles* (World Scientific, Singapore, 2005).
[7] E. Cremmer *et al.*, Phys. Lett. **79B**, 231 (1978); Nucl. Phys. **B147**, 105 (1979); R. Barbieri, S. Ferrara, and C. A. Savoy, Phys. Lett. **119B**, 343 (1982); A. H. Chamseddine, R. L. Arnowitt, and P. Nath, Phys. Rev. Lett. **49**, 970 (1982); L. J. Hall, J. D. Lykken, and S. Weinberg, Phys. Rev. D **27**, 2359 (1983); P. Nath, R. L. Arnowitt, and A. H. Chamseddine, Nucl. Phys. **B227**, 121 (1983); N. Ohta, Prog. Theor. Phys. **70**, 542 (1983).
[8] C. F. Berger, J. S. Gainer, J. L. Hewett, and T. G. Rizzo, J. High Energy Phys. 02 (2009) 023; J. Edsjo, E. Lundstrom, S. Rydbeck, and J. Sjolin, J. High Energy Phys. 03 (2010) 054; N. Ozturk (ATLAS and CMS Collaborations), arXiv:0910.2964; B. Bhattacherjee, A. Kundu, S. K. Rai, and S. Raychaudhuri, Phys. Rev. D **81**, 035021 (2010); H. Baer, S. Kraml, A. Lessa, and S. Sekmen, J. High Energy Phys. 02 (2010) 055; M.-H. Genest (CMS and ATLAS Collaborations), Proc. Sci., EPS-HEP2009 (2009) 221; D. Feldman, G. Kane, R. Lu, and B. D. Nelson, Phys. Lett. B **687**, 363 (2010); H. K. Dreiner, M. Kramer, J. M. Lindert, and B. O'Leary, J. High Energy Phys. 04, (2010) 109.
[9] A. Djouadi, M. Drees, and J. L. Kneur, J. High Energy Phys. 08 (2001) 055; J. R. Ellis, K. A. Olive, and Y. Santoso, New J. Phys. **4**, 32 (2002); M. E. Gomez, G. Lazarides, and C. Pallis, Nucl. Phys. **B638**, 165 (2002); H. Baer *et al.*, J. High Energy Phys. 07 (2002) 050; A. Djouadi, M. Drees, and J.-L. Kneur, J. High Energy Phys. 03 (2006) 033; S. Heinemeyer, X. Miao, S. Su, and G. Weiglein, J. High Energy Phys. 08 (2008) 087.
[10] O. Buchmueller *et al.*, Eur. Phys. J. C **64**, 391 (2009); **71**, 1583 (2011).
[11] M. Drees and M. M. Nojiri, Phys. Rev. D **47**, 376 (1993); G. Jungman, M. Kamionkowski, and K. Griest, Phys. Rep. **267**, 195 (1996); P. Nath and R. L. Arnowitt, Phys. Rev. D **56**, 2820 (1997); V. D. Barger and C. Kao, *ibid.* 57, 3131 (1998); G. Bertone, D. Hooper, and J. Silk, Phys. Rep. **405**, 279 (2005); H. Baer, A. Mustafayev, E.-K. Park, S. Profumo, and X. Tata, J. High Energy Phys. 04 (2006) 041; U. Chattopadhyay, D. Das, and D. P. Roy, Phys. Rev. D **79**, 095013 (2009); S. Bhattacharya, U. Chattopadhyay, D. Choudhury, D. Das, and B. Mukhopadhyaya, *ibid.* **81**, 075009 (2010).
[12] G. Bhattacharyya, arXiv:hep-ph/9709395; H. K. Dreiner, arXiv:hep-ph/9707435; S.-L. Chen, D. K. Ghosh, R. N. Mohapatra, and Y. Zhang, J. High Energy Phys. 02 (2011) 036.
[13] E. Komatsu *et al.*, Astrophys. J. Suppl. Ser. **192**, 18 (2011).
[14] ATLAS Collaboration, Report No. ATL-PHYS-PUB-2010-010, 2010.
[15] CMS Collaboration, CMS NOTE, Report No. 2010/008, 2010.
[16] H. Baer, V. Barger, A. Lessa, and X. Tata, J. High Energy Phys. 06 (2010) 102; N. Bhattacharyya, A. Datta, and S. Poddar, Phys. Rev. D **82**, 035003 (2010); B. Altunkaynak, M. Holmes, P. Nath, B. D. Nelson, and G. Peim, Phys. Rev. D **82**, 115001 (2010); N. Chen, D. Feldman, Z. Liu, P. Nath, and G. Peim, Phys. Rev. D **83**, 035005 (2011); S. Bornhauser, M. Drees, S. Grab, and J. S. Kim, Phys. Rev. D **83**, 035008 (2011).
[17] G. Kane, in *Kane*, edited by Gordon *et al.*, Perspectives on LHC Physics (2008), pp. 1–11.
[18] J. Laiho, E. Lunghi, and R. S. Van deWater, Phys. Rev. D **81**, 034503 (2010).

[19] M. Bona *et al.* (UTfit Collaboration), Phys. Lett. B **687**, 61 (2010).

[20] J. Charles *et al.* (CKMfitter Group), Eur. Phys. J. C **41**, 1 (2005).

[21] E. Barberio *et al.* (Heavy Flavor Averaging Group), arXiv:0808.1297.

[22] F. Mahmoudi, AIP Conf. Proc. **1078**, 243 (2009).

[23] B. Aubert *et al.* (*BABAR* Collaboration), Phys. Rev. D **81**, 051101 (2010).

[24] P. del Amo Sanchez *et al.* (*BABAR* Collaboration), arXiv:1008.0104.

[25] K. Hara *et al.* (Belle Collaboration), Phys. Rev. D **82**, 071101 (2010).

[26] K. Ikado *et al.* (Belle Collaboration), Phys. Rev. Lett. **97**, 251802 (2006).

[27] S. T'Jampens (CKMFitter Collaboration), ICHEP 2010, http://indico.cern.ch/getFile.py/access?contribId=190&sessionId=53&resId=0&materialId=slides&confId=73513.

[28] G. Isidori and P. Paradisi, Phys. Lett. B **639**, 499 (2006).

[29] J. R. Ellis, S. Heinemeyer, K. A. Olive, A. M. Weber, and G. Weiglein, J. High Energy Phys. 08 (2007) 083.

[30] W.-S. Hou, Phys. Rev. D **48**, 2342 (1993).

[31] A. J. Buras, P. Gambino, M. Gorbahn, S. Jager, and L. Silvestrini, Phys. Lett. B **500**, 161 (2001).

[32] V. Lubicz and C. Tarantino, Nuovo Cimento Soc. Ital. Fis. B **123**, 674 (2008).

[33] A. G. Akeroyd and S. Recksiegel, J. Phys. G **29**, 2311 (2003).

[34] A. J. Buras, P. H. Chankowski, J. Rosiek, and L. Slawianowska, Nucl. Phys.**B659**, 3 (2003).

[35] C. Amsler *et al.* (Particle Data Group), Phys. Lett. B **667**, 1 (2008).

[36] S. Heinemeyer, Int. J. Mod. Phys. A **21**, 2659 (2006).

[37] G. W. Bennett *et al.* (Muon $g-2$ Collaboration), Phys. Rev. D **73**, 072003 (2006).

[38] J. P. Miller, E. de Rafael, and B. L. Roberts, Rep. Prog. Phys. **70**, 795 (2007).

[39] D. Eriksson, F. Mahmoudi, and O. Stal, J. High Energy Phys. 11 (2008) 035.

[40] U. Chattopadhyay and P. Nath, Phys. Rev. D **53**, 1648 (1996); Phys. At. Nucl. **65**, 2101 (2002).

[41] E. Lunghi and J. Matias, J. High Energy Phys. 04 (2007) 058; M. Misiak and M. Steinhauser, Nucl. Phys. **B764**, 62 (2007); M. Misiak *et al.*, Phys. Rev. Lett. **98**, 022002 (2007); A. Freitas and U. Haisch, Phys. Rev. D **77**, 093008 (2008).

[42] D. Asner *et al.* (Heavy Flavor Averaging Group), arXiv:1010.1589.

[43] P. Nath and R. L. Arnowitt, Phys. Lett. B **336**, 395 (1994).

[44] CDF Collaboration, CDF Public Note Report No. 9892, 2009.

[45] E. Lunghi, W. Porod, and O. Vives, Phys. Rev. D **74**, 075003 (2006).

[46] A. Djouadi, J.-L. Kneur, and G. Moultaka, Comput. Phys. Commun. **176**, 426 (2007).

[47] F. Mahmoudi, Comput. Phys. Commun. **178**, 745 (2008); **180**, 1579 (2009).

[48] G. Belanger, F. Boudjema, A. Pukhov, and A. Semenov, Comput. Phys. Commun. **149**, 103 (2002); **176**, 367 (2007).

[49] M. S. Carena and H. E. Haber, Prog. Part. Nucl. Phys. **50**, 63 (2003).

[50] V. A. Bednyakov, S. G. Kovalenko, H. V. Klapdor-Kleingrothaus, and Y. Ramachers, Z. Phys. A **357**, 339 (1997); V. A. Bednyakov, H. V. Klapdor-Kleingrothaus, and S. G. Kovalenko, Phys. Rev. D **55**, 503 (1997); A. Bottino, F. Donato, N. Fornengo, and S. Scopel, *ibid.* **63**, 125003 (2001); V. A. Bednyakov, H. V. Klapdor-Kleingrothaus, and V. Gronewold, *ibid.* **66**, 115005 (2002); J. R. Ellis, K. A. Olive, Y. Santoso, and V. C. Spanos, *ibid.* **69**, 015005 (2004); L. S. Stark, P. Hafliger, A. Biland, and F. Pauss, J. High Energy Phys. 08 (2005) 059; L. Calibbi, Y. Mambrini, and S. K. Vempati, J. High Energy Phys. 09 (2007) 081; U. Chattopadhyay, D. Das, A. Datta, and S. Poddar, Phys. Rev. D **76**, 055008 (2007).

[51] A. Djouadi, M. M. Muhlleitner, and M. Spira, Acta Phys. Pol. B **38**, 635 (2007).

[52] J. Dietrich (ATLAS Collaboration), arXiv:1005.2034.

[53] V. Berezinsky *et al.*, Astropart. Phys. **5**, 1 (1996).

[54] J. R. Ellis, K. A. Olive, and Y. Santoso, Phys. Lett. B **539**, 107 (2002); J. R. Ellis, T. Falk, K. A. Olive, and Y. Santoso, Nucl. Phys. **B652**, 259 (2003); H. Baer, A. Mustafayev, S. Profumo, A. Belyaev, and X. Tata, J. High Energy Phys. 07 (2005) 065; J. Ellis, K. A. Olive, and P. Sandick, New J. Phys. **11**, 105015 (2009).